Journal of Sound and Vibration (1999) **219**(2), 265–277
Article No. jsvi.1998.1874, available online at http://www.idealibrary.com.on IDEAL

ACCURATE FREE VIBRATION ANALYSIS OF POINT SUPPORTED MINDLIN PLATES BY THE SUPERPOSITION METHOD

D. J. GORMAN

Department of Mechanical Engineering, University of Ottawa,
770 *King Edward Avenue, Ottawa, Canada K1N 6N5*

(*Received* 15 *December* 1997, *and in final form* 15 *July* 1998)

The superposition method is exploited to obtain free vibration eigenvalues for thick Mindlin plates resting on point supports. The Mindlin governing differential equations are satisfied exactly and boundary conditions are satisfied to any desired degree of accuracy by taking more terms in the solution series. Very good agreement is obtained with published results based on thin plate theory when the thickness ratio of the Mindlin plates is allowed to take on values characteristic of thin plates. Eigenvalues are tabulated for a square plate resting on four point supports distributed symmetrically along the plate diagonals. Significant differences are encountered for higher modes when eigenvalues computed by the Mindlin theory are compared with those based on the thin plate theory.

1. INTRODUCTION

The free vibration behavior of thin isotropic rectangular plates resting on point supports is a subject which has received considerable attention in recent years. In addition to being a problem of academic interest many applications of point supported plates are found in industry. Examples are to be found in bridge decks, the mounting of solar panels, and in electronic circuit board design.

Among the literature relevant to point supported thin plates is an earlier publication by Gorman [1], as well as subsequent publications by Raju and Amba-Rao [2], and Narita [3]. In a later publication Gorman [4] showed that very good agreement was encountered when the computed results of all the above publications were compared. Other related technical papers were listed by Gorman [1].

One can conclude, therefore, that the problem of computing resonant frequencies and mode shapes for point supported thin isotropic rectangular plates is fully resolved. It is know, however, that the situation pertaining to thick plates, or even thin plates with low resistance to deformation induced by transverse shear stress, is quite different. The objective set forth in this paper is to describe the method employed and the results obtained when a free vibration analysis was conducted on point supported thick Mindlin plates. The superposition method

0022–460X/99/020265 + 13 $30.00/0

was employed to obtain a solution for the governing Mindlin equations. Verification of the method was carried out by comparing thin plate, and thick plate results, as the thickness ratio of the Mindlin plate was allowed to take on values characteristic of thin rectangular plates.

2. MATHEMATICAL PROCEDURE

The analysis is carried out through superposition of the five forced vibration solutions (building blocks) shown schematically in Figure 1. The first four building blocks were utilized earlier by Gorman [5] in analyzing the free vibration of completely free thick Mindlin plates. They were described in detail in this earlier publication and hence, only a brief description of their development will be given here for the sake of completeness. In fact, the present solution constitutes essentially an extension of the earlier solution pertaining to the completely free Mindlin plate.

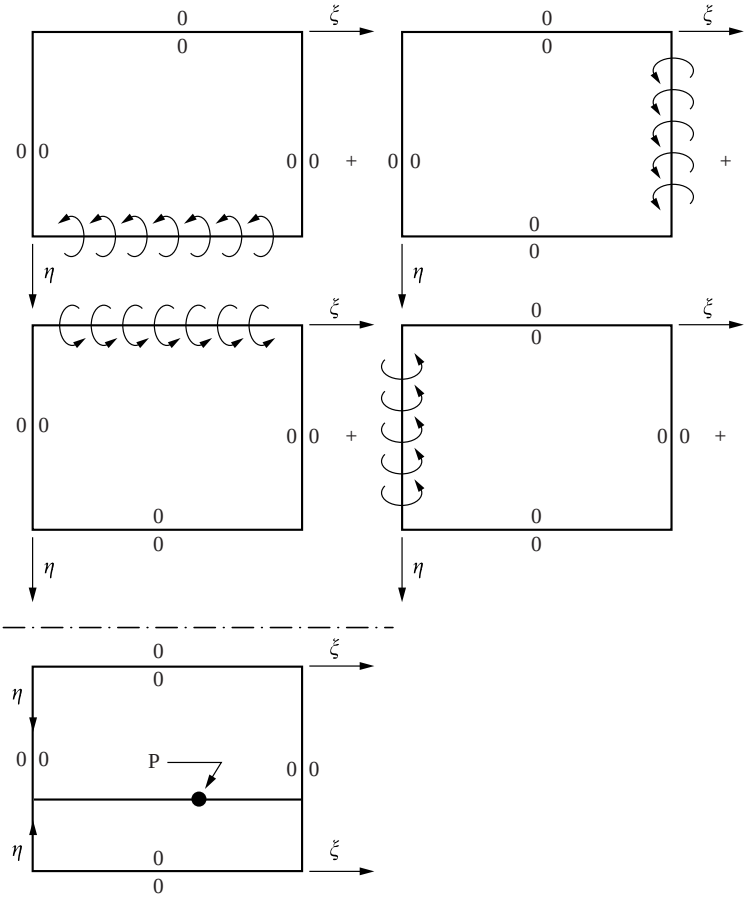

Figure 1. Schematic representation of building blocks utilized in analyzing free vibration of point supported Mindlin plates.

2.1. DEVELOPMENT OF THE FIRST BUILDING BLOCK

The three governing differential equations controlling the vibratory behavior of Mindlin plates are written in dimensionless form as

$$\frac{\partial^2 W}{\partial \xi^2} + \frac{1}{\phi^2}\frac{\partial^2 W}{\partial \eta^2} + \frac{\partial \psi_\eta}{\partial \eta} + \frac{\lambda^4 \phi_h^2}{v_3} W = 0, \tag{1}$$

$$\frac{\partial^2 \psi_\xi}{\partial \xi^2} + \frac{v_1}{\phi^2}\frac{\partial^2 \psi_\xi}{\partial \eta^2} + \frac{v_2}{\phi}\frac{\partial^2 \psi_\eta}{\partial \xi\, \partial \eta} - \frac{v_3}{\phi_h^2}\left(\psi_\xi + \frac{\partial W}{\partial \xi}\right) + \frac{\lambda^4 \phi_h^2}{12}\psi_\xi = 0, \tag{2}$$

$$\frac{\partial^2 \psi_\eta}{\partial \xi^2} + \frac{1}{\phi^2 v_1}\frac{\partial^2 \psi_\eta}{\partial \eta^2} + \frac{v_2}{\phi \eta_1}\frac{\partial^2 \psi_\xi}{\partial \xi\, \partial \eta} - \frac{v_3}{\phi_h^2 v_1}\left(\psi_\eta + \frac{1}{\phi}\frac{\partial W}{\partial \eta}\right) + \frac{\lambda^4 \phi_h^2}{12 v_1}\psi_\eta = 0. \tag{3}$$

Shear forces, bending moments, and twisting moments in dimensionless form are written as

$$Q_\xi = \psi_\xi + \frac{\partial W}{\partial \xi}, \qquad Q_\eta = \psi_\eta + \frac{1}{\phi}\frac{\partial W}{\partial \eta},$$

$$M_\xi = \frac{\partial \psi_\xi}{\partial \xi} + \frac{v}{\phi}\frac{\partial \psi_\eta}{\partial \eta}, \qquad M_\eta = \frac{\partial \psi_\eta}{\partial \eta} + v\phi\frac{\partial \psi_\xi}{\partial \xi}, \qquad M_{\xi\eta} = \frac{\partial \psi_\eta}{\partial \xi} + \frac{1}{\phi}\frac{\partial \psi_\xi}{\partial \eta}. \tag{4}$$

The first building block of Figure 1 has slip-shear conditions imposed along the three non-driven edges. These conditions, indicated by two small circles adjacent to the boundary, imply zero transverse shear force as well as zero twisting moment along the edge. They also imply zero rotation of the plate cross-section about a mid-plane line running parallel to the edge.

The driven edge is free of transverse shear force and twisting moment. It is driven by a distributed harmonic bending moment. The amplitude of this moment is represented in series form as

$$M_\eta = \sum_{m=1,2}^{\infty} E_m \cos{(m-1)\pi\xi}. \tag{5}$$

We begin by considering the response of the building block to the first Fourier term of equation (5). Only the lateral displacement W and the parameter ψ_η will be non-zero. Both will be functions of η, only. The governing differential equations reduce to a set of two,

$$\frac{\mathrm{d}^2 W}{\mathrm{d}\eta^2} + \phi^2\frac{\mathrm{d}\psi_\eta}{\mathrm{d}\eta} + \frac{\lambda^4 \phi^2 \phi_h^2 W}{v_3} = 0 \tag{6}$$

and

$$\frac{\mathrm{d}^2 \psi_\eta}{\mathrm{d}\eta^2} - \frac{v_3 \phi^2}{\phi_h^2}\left(\psi_\eta + \frac{1}{\phi}\frac{\mathrm{d}W}{\mathrm{d}\eta}\right) + \frac{\lambda^4 \phi^2 \phi_h^2 \psi_\eta}{12} = 0. \tag{7}$$

Denoting the functions $W(\eta) = X(\eta)$, and $\psi_\eta(\eta) = Z(\eta)$, we substitute them into the pair of equilibrium equations. After operating on these equations with

appropriate operators, the quantity $Z(\eta)$ is eliminated, leaving a single ordinary differential equation of the form

$$\{D^4 + \alpha_{11}D^2 + \alpha_{22}\}X(\eta) = 0, \tag{8}$$

where the symbol D represents the differential operator and α_{11} and α_{22} are known quantities. Denoting the squares of the roots of the characteristic equation associated with the above differential equation as R_1 and R_2, it is found that they are always real for our range of interest. Three forms of solution are possible. They are

$$\text{Case 1, } R_1,\ R_2 < 0{\cdot}0; \quad \text{Case 2, } R_1 < 0{\cdot}0,\ R_2 > 0{\cdot}0; \quad \text{Case 3, } R_1,\ R_2 > 0{\cdot}0. \tag{9}$$

Let us set

$$\alpha\sqrt{|R_1|}, \qquad \beta = \sqrt{|R_2|}. \tag{10}$$

Considering Case 1, for example, and taking advantage of symmetry about the ξ-axis, and enforcing boundary conditions at the edge, $\eta = 1$, the solution takes the form

$$X(\eta) = \frac{E_1}{X2}(\cos \alpha\eta + X1 \cos \beta\eta), \tag{11}$$

and returning to the coupling equation one can write

$$Z(\eta) = \frac{E_1}{X2}(S_{m1} \sin \alpha\eta + X1S_{m2} \sin \beta\eta), \tag{12}$$

Similar forms of solution are available for the other two cases. All symbols are defined in the publication by Gorman [5].

We next look at the building block response to Fourier terms where $m > 1$. Lévy type solutions for the three parameters of interest are written as

$$W(\xi, \eta) = \sum_{m=2,3}^{\infty} X_m(\eta) \cos (m-1)\pi\xi,$$

$$\psi_\xi(\xi, \eta) = \sum_{m=2,3}^{\infty} Y_m(\eta) \sin (m-1)\pi\xi, \quad \psi_\eta(\xi, \eta) = \sum_{m=2,3}^{\infty} Z_m(\eta) \cos (m-1)\pi\xi. \tag{13–15}$$

The next step is to substitute these expressions into the three governing differential equations. One thereby obtains a set of three coupled ordinary differential equations. Again, utilizing appropriate differential operators, the function $X_m(\eta)$ and $Z_m(\eta)$ may be eliminated and a sixth order ordinary differential equation involving $Y_m(\eta)$, only, is obtained. It is written as

$$\{D^6 + \alpha_{11}D^4 + \alpha_{22}D^2 + \alpha_{33}\}Y_m(\eta) = 0. \tag{16}$$

Now we set the squares of the roots of the associated characteristic equation equal to R_1, R_2, and R_3, and it is found that all three are real for our range of interest. We introduce the quantities

$$\alpha = \sqrt{|R_1|}, \qquad \beta = \sqrt{|R_2|}, \qquad \gamma = \sqrt{|R_3|} \tag{17}$$

and it becomes apparent that four possible forms of solution exist. They are described as,

$$\text{Case 1, } R_1, R_2 \text{ and } R_3 < 0{\cdot}0; \quad \text{Case 2, } R_1, R_2 < 0{\cdot}0, R_3 > 0{\cdot}0;$$

$$\text{Case 3, } R_1 < 0{\cdot}0, R_2, R_3 > 0{\cdot}0; \quad \text{Case 4, } R_1, R_2 \text{ and } R_3 > 0{\cdot}0. \tag{18}$$

For illustrative purposes only the solution for Case 1 will be examined. After taking advantage of symmetry about the ξ-axis, and thereby eliminating three of the unknowns, the solution is obtained in the form

$$Y_m(\eta) = A_m \cos \alpha\eta + B_m \cos \beta\eta + C_m \cos \gamma\eta. \tag{19}$$

Upon enforcing the boundary conditions along the driven edge one obtains

$$Y_m(\eta) = \frac{E_m}{X3}\{\cos \alpha\eta + X1 \cos \beta\eta + X2 \cos \gamma\eta\}. \tag{20}$$

Returning to the coupling equations from which the parameter $Y_m(\eta)$ was separated it is easily shown that one may write

$$X_m(\eta) = \frac{E_m}{X3}\{R_{m1} \cos \alpha\eta + X1\ R_{m2} \cos \beta\eta + X2\ R_{m3} \cos \gamma\eta\} \tag{21}$$

and

$$Z_m(\eta) = \frac{E_m}{X3}\{S_{m1} \sin \alpha\eta + X1\ S_{m2} \sin \beta\eta + X2\ S_{m3} \cos \gamma\eta\}. \tag{22}$$

Again, all symbols are as defined in the publication by Gorman [5]. Solutions for Cases 2, 3, etc., differ from that given above in that some or all of the trigonometric functions will be replaced by hyperbolic functions. In fact, for all work reported here, only Cases 3 and 4 are encountered for the higher Fourier driving coefficients.

One thus has available the exact response of the first building block to any number of terms in the driving series. It will be appreciated that solutions for the second, third, and fourth building blocks of Figure 1 are readily extracted from the above solution by an interchange of axis, or replacing the parameter η by $1 - \eta$ or ξ by $1 - \xi$, etc. The rules for transformation of axes when altering the solution for the first building block in order to obtain the solution for the second, for example, are summarized in an earlier publication [5]. They are repeated here for convenience. (1) Temporarily replace λ^2 with $\lambda^2\phi^2$. (2) Replace ϕ_h by ϕ_h/ϕ. (3) Temporarily replace ϕ with its inverse, $1/\phi$. (4) It is customary to replace the previous subscript "m", with "n", in order to avoid confusion.

2.2. DEVELOPMENT OF THE FIFTH BUILDING BLOCK SOLUTION

A solution for this building block response is obtained by following the same basic approach as that utilized so often in thin plate theory. The present transverse-shear deformable building block is given slip-shear support, as defined earlier, along all edges. It is driven by a harmonic concentrated force acting on the lateral surface at dimensionless co-ordinates u and v, with respect to the upper reference frame.

The building block is considered to be composed of two rectangular plate segments, each with a separate co-ordinate system. The common boundary runs parallel to the ξ-axis and passes through the point of application of the driving force. The amplitude of this dimensionless force is represented by a Dirac function running along the common boundary. This function, in turn, is represented in series form. Before non-dimensionalizing, the condition of lateral force equilibrium across the common boundary is written as

$$\kappa^2 Gh\left[\frac{\partial W_1(x, y)}{\partial y} + \frac{\partial W_2(x, y)}{\partial y}\right] = \frac{2P}{a} \sum_{m=1,2}^{\infty} \frac{\cos(m-1)\pi u}{\delta_m} \cos(m-1)\pi \frac{x}{a}, \quad (23)$$

where $\delta_m = 2$, $m = 1$; $\delta_m = 1$, $m > 1$, and the subscripts 1, and 2, refer to the upper and lower segments of the building block, respectively.

We begin by considering the response of this building block to the first driving term on the right hand side of equation (23), that is, the case where $m = 1$. Again the response will be a function of the co-ordinate η, only. Referring to the earlier solution, and concentrating on the situation of Case 2, we will again replace the functions $W_1(\eta)$, and $\psi_1(\eta)$ with $X_1(\eta)$ and $Z_1(\eta)$, respectively. A similar set of functions with subscript 2 will pretain to the lower segment of the building block.

It will be obvious that the above functions, after enforcing the outer boundary conditions, must take the form [5]

$$X_1(\eta) = A_{m1} \cos \alpha\eta + B_{m1} \cosh \beta\eta$$

and

$$Z_1(\eta) = A_{m1} S_{m1} \sin \alpha\eta + B_{m1} S_{m2} \sinh \beta\eta, \quad (24)$$

where α and β are defined in equation (10), and quantities S_{m1} and S_{m2} are obtained through coupling of equations (6) and (7). A similar set of solutions with subscript 2 exist for the lower segment of the building block.

Conditions of continuity which must be enforced across the common boundary are those of displacement, cross-section rotation, moment, and shear force–transverse driving force equilibrium (equation (23)). The latter is expressed in dimensionless form as

$$\left.\frac{dX_1(\eta)}{d\eta}\right|_{\eta=v} + \left.\frac{dX_2(\eta)}{d\eta}\right|_{\eta=v^*} = \frac{P^*}{2}. \quad (25)$$

It follows immediately that the set of four simultaneous non-homogenous equations resulting from enforcement of the above continuity conditions may be represented schematically as indicated below. These equations are readily solved by a simple computer routine to obtain values for the four unknowns in terms of the dimensionless driving force amplitude, P^*.

$$\begin{matrix} A_{m1} & B_{m1} & A_{m2} & B_{m2} \end{matrix}$$

$$\begin{bmatrix} \cos \alpha v & \cosh \beta v & -\cos \alpha v^* & -\cosh \beta v^* \\ S_{mi} \sin \alpha v & S_{m2} \sinh \beta v & S_{mi} \sin \omega^* & S_{mi} \sinh \beta v^* \\ S_{mi}\alpha \cos \alpha v & S_{m2}\beta \cosh \beta v & -S_{mi}\alpha \cos \alpha v^* & -S_{m2} \cosh \beta v^* \\ -\alpha \sin \alpha v & \beta \sinh \beta v & -\alpha \sin \alpha v^* & \beta \sinh \beta v^* \end{bmatrix} = \begin{bmatrix} 0 \\ 0 \\ 0 \\ P^*/2 \end{bmatrix}. \tag{26}$$

Next the building block response to higher driving terms in the series, i.e., $m > 1$, is examined. Again the quantities W, ψ_η, etc., take the form given by equations (13–15). The functions $X_m(\eta)$, $X_m(\eta)$, etc., after enforcing the boundary conditions at the boundaries, $\eta = 0$, become [5]

$$X(\eta) = A_m R_{m1} \cos \alpha\eta + B_m R_{m2} \cosh \beta\eta + C_m R_{m3} \cosh \gamma\eta, \tag{27}$$

$$Y(\eta) = A_m \cos \alpha\eta + B_m \cosh \beta\eta + C_m \cosh \gamma\eta, \tag{28}$$

$$Z(\eta) = A_m S_{m1} \sin \alpha\eta + B_m S_{m2} \sinh \beta\eta + C_m S_{m3} \sinh \gamma\eta, \tag{29}$$

The six conditions of continuity to be enforced across the common boundary, along with their appropriate mathematical formulation, are (superscripts indicate differentiation with respect to η)

(1) Continuity of $W(\xi, \eta)$; require $X_1(\eta)|_{\eta = v} = X_2(\eta)|_{\eta = v^*}$.
(2) Continuity of $\psi_\eta(\xi, \eta)$; require $Z_1(\eta)|_{\eta = v} = -Z_2(\eta)|_{\eta = v^*}$.
(3) Continuity of $M_\eta(\xi, \eta)$; require $Z_1'(\eta)|_{\eta = v} = Z_2'(\eta)|_{\eta = v^*}$.
(4) Continuity of $M_{\eta\xi}(\xi, \eta)$; require $Y_1'(\eta)|_{\eta = v} = -Y_2'(\eta)|_{\eta = v^*}$.
(5) Continuity of $\psi_\xi(\xi, \eta)$; require $Y_1(\eta)|_{\eta = v} = Y_2(\eta)|_{\eta = v^*}$.
(6) Require $Q_1'(\eta)|_{\eta = v} + Q_\eta(\xi, \eta)|_{\eta = v^*} = P^* \cos (m - 1)\pi u$, $\therefore$ require $X_1'(\eta)|_{\eta = v} + X_2'(\eta)|_{\eta = v^*} = P^* \cos (m - 1)\pi u$.

It is seen that the above continuity conditions provide a set of six non-homogenous equations for evaluation of the unknowns A_{m1}, B_{m1}, . . . etc. Again, these unknowns are readily evaluated with a simple computer sub-routine. We now have a solution for the response of the fifth building block to any harmonic driving force of dimensionless amplitude P^*. It is appropriate at this time to point out that this solution for the fifth building block is valid, regardless of the driving force location, i.e., it may be located anywhere on the interior surface of the plate or on the plate edges. The fact that the solution is valid, for example, even when the co-ordinates u or v take on extreme values of zero or one, was not appreciated in earlier publications utilizing the superposition method for thin plate analysis. In fact, separate solutions developed earlier for plates driven by concentrated forces along their edges were not really necessary.

3. GENERATION OF THE EIGENVALUE MATRIX

This part of the procedure is virtually identical to that described earlier for analysis of point supported thin plates. In addition to the first four building blocks we will require an additional building block of the type described immediately above for each point support acting on the plate of interest. It will be obvious that all required edge conditions of the superimposed set of building blocks are satisfied except that of zero bending moment along the boundaries. Furthermore, the condition that the net displacement at the location of all point supports should equal zero, must also be satisfied.

A schematic representation of a typical eigenvalue matrix is presented in Figure 2. Here, only a single point support is considered to act. Small inserts to the right of the figure indicate boundary conditions to be satisfied.

In the upper segment of the matrix we require vanishing of the net bending moment along the edge, $\eta = 1$. Toward this end the sum of the contributions of each building block toward the bending moment along this edge is expanded in a cosine series of K terms where K equals the number of terms in the building block expansions. Each coefficient in this new series is set equal to zero, thereby providing a set of K homogenous algebraic equations relating the Fourier driving coefficients and the driving force dimensionless amplitude. It will be noted that

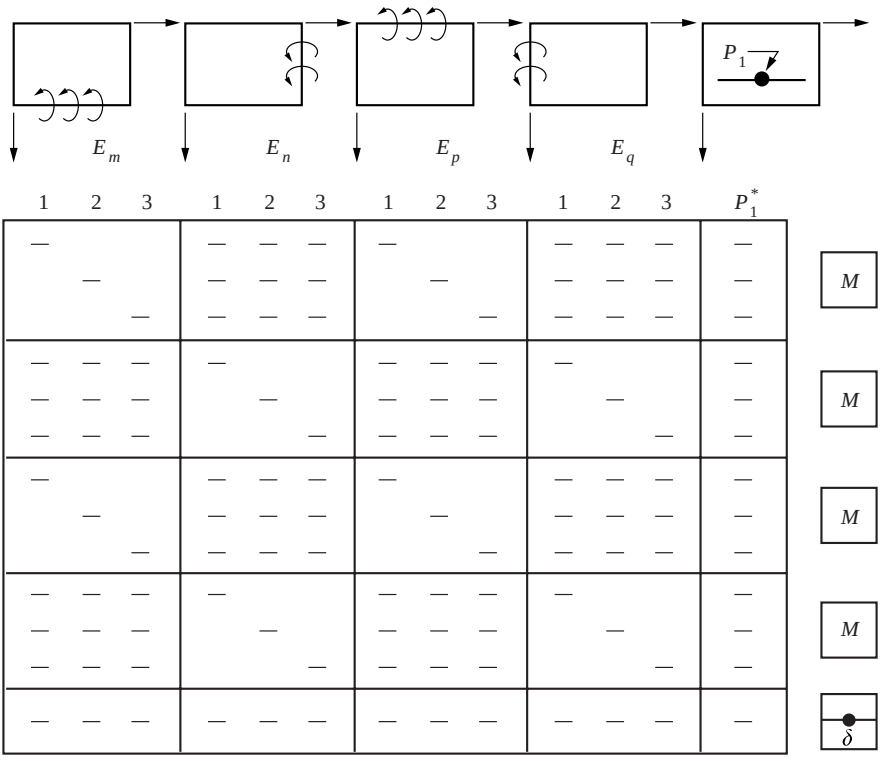

Figure 2. Schematic representation of eigenvalue matrix based on three term building block solutions

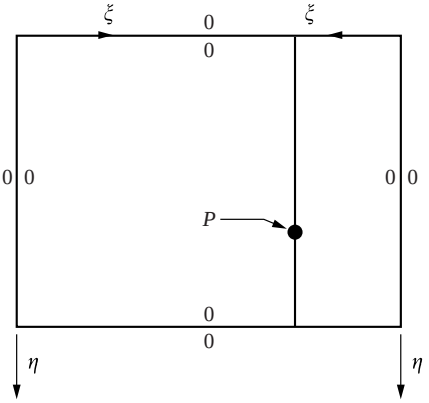

Figure 3. Alternate building block driven by concentrated harmonic driving force. Dirac function lies along line running parallel to η-axis.

the contribution to bending moment of the point-force driven building block is already available in the form of a cosine series.

Moving down to the edge, $\xi = 1$, we find that the contribution toward bending moment of this latter building block is not directly available in series form. Experience has shown that the best means for handling this contribution is to follow the same procedure as that followed for thin plates in an earlier publication [1].

We re-consider the formulation of the point-force driven building block for Figure 1. Let us suppose the building block is divided into two segments by a partition line running parallel to the η-axis, as shown in Figure 3. The solution for the response of this building block can obviously be obtained from the companion solution of Figure 1 through introducing an interchange of axes as discussed earlier. In addition to introducing the transformation modifications, u must now be replaced with v, and v with u. In view of the original definition of P^*, P^* must now be temporarily replaced with P^*/ϕ^4, as discussed in an earlier publication [6]. With this new solution to the same building block, one has its contributions toward bending moment along edges, $\xi = 1$, and $\xi = 0$, available in cosine series form. Thus it is possible to complete generation of the first four segments of the matrix of Figure 2.

Finally, it is required that net displacement at each point support must vanish. Thus a set of homogenous algebraic equations equal to the number of driving unknowns is obtained. Then, those values of the parameter λ^2 which cause the determinant of the eigenvalue matrix to vanish i.e., the eigenvalues, are searched for. Mode shapes associated with each eigenvalue are obtained after setting one of the non-zero unknowns equal to unity and solving the resulting set of non-homogenous equations for the remaining unknowns.

It is important to note that each additional support point necessitates the addition of only one more row and one more column to the matrix. Numerous point supports can therefore be handled without serious difficulty.

4. PRESENTATION OF RESULTS

It will be understood that no attempt can be made to store eigenvalues to cover all possible design needs. Accordingly, only a limited amount of data is presented to demonstrate the method and to permit validation tests.

In a paper referred to earlier [4], a thorough study was made of the free vibration of thin square rectangular plates resting on four symmetrically distributed point supports acting on the diagonals. The first four eigenvalues were listed for plates in symmetric–symmetric, anti-symmetric–anti-symmetric, and symmetric–anti-symmetric modes. It was decided to follow the same type of study here, utilizing the Mindlin thick plate theory. Two plate thickness ratios were utilized, 0·01 and 0·1. It is known that with the ratio of 0·01, which corresponds to a thin plate, the Mindlin theory should generate eigenvalues which are almost equal, though probably slightly below those computed by thin plate theory. This slight reduction is to be expected as the Mindlin theory, unlike the thin plate theory, takes plate rotary inertia into account and does not consider the ability of the plate to resist transverse shear force induced deformation to be infinite. This type of comparison provides a valuable check on the Mindlin theory and its application.

Results of the earlier thin plate study, as well as eigenvalues computed here by the Mindlin theory, for two plate thickness ratios, are presented in Tables 1–3. These results pertain to the three families of free vibration modes as discussed earlier. It shoud be made clear that while the thin plate eigenvalues were computed by focusing on a quarter plate only, the current results, based on Mindlin theory, were computed by utilizing the full plate analysis as described in this paper.

TABLE 1

Computed eigenvalues for fully symmetric mode vibration of square plate with four supports symmetrically distributed on diagonals ($v = 0{\cdot}333$); u, v, *provide co-ordinates of one point support*

	$u = v$									
Mode	0	0·05	0·1	0·15	0·2	0·25	0·3	0·35	0·4	
	7·112	9·464	12·81	17·59	19·22	19·22	19·22	15·72	13·37	A*
1	7·078	9·448	12·80	17·58	19·22	19·22	19·22	15·72	13·37	B
	6·666	9·033	12·19	16·59	18·58	18·58	18·58	14·97	12·75	C
	19·22	19·22	19·22	19·22	23·12	23·54	19·26	19·22	19·22	A
2	19·22	19·22	19·22	19·22	23·10	23·53	19·25	19·22	19·22	B
	18·58	18·58	18·58	18·58	21·98	22·51	18·28	18·58	18·58	C
	44·08	49·44	54·04	57·32	54·56	55·08	59·56	56·64	52·56	A
3	43·76	49·17	53·75	57·05	54·33	54·86	59·19	56·32	52·27	B
	38·59	43·52	47·09	48·56	40·29	40·06	48·94	48·40	45·42	C
	91·56	110·4	116·4	87·12	63·88	63·16	81·20	116·4	110·5	A
4	91·02	110·0	116·1	87·68	63·51	62·81	80·94	116·1	110·1	B
	75·36	91·05	97·61	66·09	55·22	55·05	60·57	97·61	87·72	C

*A: Thin plate theory [4]; B: $\phi_h = 0{\cdot}01$; C: $\phi_h = 0{\cdot}1$.

TABLE 2

Computed eigenvalues for fully antisymmetric mode vibration of square plate with four supports symmetrically distributed on diagonals ($v = 0{\cdot}333$); u, v, *provide co-ordinates of one point support*

	$u = v$									
Mode	0	0·05	0·1	0·15	0·2	0·25	0·3	0·35	0·4	
	38·18	50·56	66·52	68·12	51·04	34·81	25·38	19·53	15·88	A*
1	37·96	50·36	66·34	67·82	50·82	34·65	25·26	19·44	15·81	B
	33·11	44·17	56·79	59·63	40·29	27·95	20·64	16·18	13·64	C
	68·12	68·12	68·12	75·44	68·12	68·12	68·12	68·12	68·12	A
2	67·82	67·82	67·82	75·16	67·82	67·82	67·82	67·82	67·82	B
	59·63	59·63	59·63	62·90	59·63	59·63	59·63	59·63	59·63	C
	121·8	138·7	145·5	109·3	122·7	123·1	110·6	97·12	86·32	A
3	120·9	138·1	144·4	108·6	121·8	122·1	109·8	96·55	85·90	B
	97·61	109·4	107·1	72·50	97·61	91·44	85·12	77·35	71·17	C
	173·2	199·5	188·3	151·6	157·6	198·2	202·6	188·3	169·6	A
	172·0	198·9	186·6	150·5	156·6	197·2	201·4	186·9	168·2	B
	131·9	149·4	126·2	119·3	121·9	139·6	153·7	136·8	125·1	C

*A: Thin plate theory [4]; B: $\phi_h = 0{\cdot}01$; C: $\phi_h = 0{\cdot}1$.

TABLE 3

Computed eigenvalues for symmetric–antisymmetric mode vibration of square plate with four supports symmetrically distributed on diagonals ($v = 0{\cdot}333$); u, v, *provide co-ordinates of one point support*

	$u = v$									
Mode	0	0·05	0·1	0·15	0·2	0·25	0·3	0·35	0·4	
	15·55	19·23	23·39	27·79	31·77	32·61	23·58	17·72	13·53	A*
1	15·54	19·14	23·29	27·69	31·66	32·53	23·53	17·68	13·50	B
	13·91	17·53	21·25	25·07	28·44	26·79	19·64	14·61	10·70	C
	49·92	54·12	58·32	60·80	47·36	34·69	36·36	36·97	36·81	A
2	49·67	54·03	58·21	60·71	47·24	34·57	36·22	36·83	36·66	B
	44·43	48·73	52·38	54·95	39·26	31·52	32·74	33·22	33·00	C
	80·08	91·20	99·16	92·92	83·36	92·88	92·32	85·96	74·44	A
3	79·60	90·71	98·58	92·88	83·05	92·45	91·74	85·50	78·10	B
	67·48	76·13	81·21	64·94	64·98	72·24	73·79	69·93	64·72	C
	115·1	121·4	130·5	104·7	104·2	106·9	122·8	130·7	126·8	A
	114·5	221·0	129·9	104·0	103·5	106·4	122·3	130·2	126·1	B
	94·28	99·32	106·5	86·74	86·61	88·02	97·48	107·4	99·15	C

*A: Thin plate theory [4]; B: $\phi_h = 0{\cdot}01$; C: $\phi_h = 0{\cdot}1$.

Results are presented for nine different support point configurations, with the first four eigenvalues tabulated for each mode family. Twenty-four terms were utilized in the building block solutions for the present study. Convergence tests indicated that eigenvalues are accurate to three significant digits and in almost all cases to four significant digits.

The most striking observation relates to the very good agreement encountered when results of the thin plate theory are compared to results obtained by the Mindlin theory for a thickness ratio of 0·01. In view of the fact that the thin plate theory results tabulated here were found to be in very good agreement with the findings of several other researchers, as discussed earlier, one is entitled to have high confidence in the present Mindlin theory results.

Moving on to results obtained here for plates with much higher thickness ratios, i.e., 0·1, the most striking observation is the vast decrease in eigenvalues associated with this thickness ratio increase. This decrease is particularly large for the higher vibration modes. Based on these results it is seen that large errors in computed natural frequencies of thick plates would be encountered for many vibration modes, particularly the higher ones, if one were to rely on thin plate theoretical analysis.

5. DISCUSSION AND CONCLUSIONS

It is found that the superposition method is ideally suited for the free vibration analysis of thick Mindlin plates resting on point supports. The supports may be given any distribution upon the plate surface or along the edges. Very good agreement is obtained between the results of the Mindlin theory and thin plate theory for low values of plate thickness ratios. The most obvious conclusion to be drawn, based on results of the study, is that thin plate theory is particularly unsuited for computing resonant frequencies of the higher modes of point-supported thick plates. Discrepancies of more than 25% would have been encountered for some of the modes studied here.

While the outer boundaries of the plates studied here were considered to be free of edge support it will be appreciated that the same method of analysis would work just as well if any of the other classical edge conditions had been imposed.

REFERENCES

1. D. J. Gorman 1981 *Journal of Sound and Vibration* **79**, 561–574. Analytical solution for the free vibration analysis of rectangular plates resting on symmetrically distributed point supports.
2. I. S. Raju and C. L. Amba-Rao 1983 *Journal of Sound and Vibration* **90**, 291–297. Free vibrations of a square plate symmetrically supported at four points on the diagonals.
3. Y. Narita 1984 *Journal of Sound and Vibration* **93**, 593–597. Note on vibrations of point supported rectangular plates.
4. D. J. Gorman 1989 *Journal of Sound and Vibration* **131**, 515–519. A note on the free vibration of rectangular plates resting on symmetrically distributed point supports.
5. D. J. Gorman 1996 *Journal of Sound and Vibration* **189**, 341–353. Accurate free vibration analysis of the completely free rectangular Mindlin plate.

6. D. J. GORMAN 1982 *Free Vibration Analysis of Rectangular Plates*. Amsterdam: Elsevier North Holland Inc.

APPENDIX: LIST OF SYMBOLS

a, b	plate edge dimensions
D	$= Eh^3/(12(1-\upsilon^2))$, plate flexural rigidity
E	Young's modulus for plate material
G	shear modulus of plate material
h	plate thickness
K	number of terms in series solutions
M_ξ, M_η	bending moments associated with ξ and η directions, respectively
$M_{\xi\eta}$	twisting moment
P	amplitude of concentrated harmonic driving force
P^*	$= -2Pb^3/Da^2$
Q_ξ, Q_η	transverse shear forces associated with ξ and η directions, respectively
u, v	dimensionless co-ordinates of point support
u^*, v^*	$= 1-u$, and $1-v$, respectively
W	plate lateral displacement divided by side length "a"
x, y	co-ordinate distance along ξ and η directions, respectively
ξ, η	distances along plate co-ordinate axes divided by a and b, respectively
λ^2	$= \omega a^2\sqrt{\rho/D}$, free vibration eigenvalue
ρ	mass of plate per unit area
ω	circular frequency of plate vibration
ϕ	$= b/a$, plate aspect ratio
ϕ_h	h/a, plate thickness ratio
ψ_ξ, ψ_η	plate cross-section rotation associated with ξ and η directions, respectively
κ^2	Mindlin shear factor
ν	Poisson ratio of plate material
ν_1	$= (1-\nu)/2$
ν_2	$= (1+\nu)/2$
ν_3	$= 6\kappa^2(1-\nu)$